Energy, Mines and Resources Canada | Énergie, Mines et Ressources Canada

CANMET

Canada Centre for Mineral and Energy Technology | Centre canadien de la technologie des minéraux et de l'énergie

CORROSION RESISTANCE OF DOLOMA BRICKS IN CONTACT WITH SLAGS FROM SECONDARY STEELMAKING

D.H.H. Quon and K.E. Bell
Mineral Processing Laboratory

May 1986

Project 3.0.2.9.05
Electrodes and Refractories for the Steel Industry

MICROMEDIA
JUL 10 1986

This document is an unedited interim report prepared primarily for circulation and internal reporting purposes. It does not represent a final expression of the opinion of the Canada Centre for Mineral and Energy Technology (CANMET)

Ce document est un rapport provisoire non-révisé et rédigé principalement pour la diffusion et la documentation internes. Il ne représente nullement l'expression définitive de l'opinion du Centre canadien de la technologie des minéraux et de l'énergie (CANMET)

MINERAL SCIENCES LABORATORIES
DIVISION REPORT MSL 86-63(IR)
32pp

CORROSION RESISTANCE OF DOLOMA BRICKS IN CONTACT WITH SLAGS FROM SECONDARY STEELMAKING

by

D.H.H. Quon* and K.E. Bell**

ABSTRACT

Corrosion resistance of direct-bonded, tar-bonded, resin-bonded and carbon-containing dolomas to slags from the steelmaking process was examined. The corrosion resistance is greater for bricks in contact with basic slag. Most dolomas exhibited excellent corrosion resistance to slag at below 1700°C. Above 1700°C substantial slag infiltration occurred, resulting in rapid degradation of the brick. The slag retardation action of the graphite is readily apparent in the carbon-containing and resin-bonded dolomas.

---

*Research Scientist and **Head, Ceramic Section, Mineral Processing Laboratory, Mineral Sciences Laboratories, CANMET, Energy, Mines and Resources Canada, Ottawa.

RÉSISTANCE À LA CORROSION DE BRIQUES DOLOMO EN CONTACT AVEC DU LAITIER RÉSULTANT DE LA FABRICATION DE L'ACIER

par

D.H. Quon* et K.E. Bell**

RÉSUMÉ

La résistance à la corrosion de dolomies à teneur en carbone, liées directement et agglomérées avec du gaudron et de la résine qui entrent en contact avec du laitier résultant du procédé de fabrication de l'acier a été étudiée. La résistance à la corrosion des briques qui sont en contact avec du laitier basique est plus élevée. La plupart des dolomies qui sont en contact avec du laitier font preuvent d'une résistance à la corrosion très élevée à une température inférieure à 1 700°C. À une température supérieure à 1 700°C, une infiltration importante de laitier se produit résultant dans la détérioration rapide de la brique. L'action de retardement du graphite sur le laitier est très apparente dans les dolomies à teneur en carbone agglomérées avec de la résine.

INTRODUCTION

The processing steps in secondary steelmaking involve decarburization, desulphurization, final alloying, etc., and are accompanied by high temperature and slag composition-changes that normally affect the refractories of the performance. Refractories wear in the VAD refining vessels at Atlas Steels Company, as reported by Whittaker and Palmer; high alumina refractories last about 28-30 heats (1). In the argon-bubbling process, the bottom of the ladle is lined with 50% alumina brick and the side-walls are of 70% alumina brick, with rebonded fused grain chrome magnesia at the slag lines. The life of the side wall lining is about 40 heats.

To improve the ladle performance it is necessary to use special refractories in the more vulnerable parts of the lining to reduce the refractories consumption (3,5,6,7). Recently, doloma refractories have been adopted to replace alumina refractories in the low-wear area of the ladles. The doloma-based refractories are not only cost effective, but also make the ladle fully basic and thereby more compatible with basic slag; hence dissolution of the refractories would not alter the slag composition appreciably. Tests conducted on the durability of doloma refractories in steel plants indicated that the lining life has increased from 34 heats with high alumina refractories to 60 heats with doloma.

Several types of doloma refractories are commercially available, based either on improved performance or low cost. The aim of this work was to examine the performance of doloma refractories in vacuum at high temperatures in contact with slags from speciality steels.

DOLOMA REFRACTORIES

Doloma is obtained by calcining dolomite [$CaMg(CO_3)_2$] at high temperature to drive off the CO_2 to form end products comprising principally CaO and MgO (2,4). Although CaO and MgO are similar in crystal structure, only limited solid solution of these two products can be formed. Significant solid solution of CaO with MgO or MgO with CaO however, can be obtained by sintering at 1800°C and 2000°C respectively (8). All naturally occurring dolomites can be calcined to make doloma refractories, but different levels of impurities

and differences in texture can markedly affect their sintering characteristics. Doloma is very hygroscopic and must be dead-burnt to as high a density as possible. The dead-burnt doloma is subjected to further processing in making the refractory brick, commonly by pressing and sintering bricks made from crushed and graded doloma aggregates in a fine-grained doloma matrix. Further treatment of the sintered doloma can be achieved by incorporating tar or resin as a bonding agent or by coating the reactive surface for retardation of the hydration process. Adding graphite flake to the doloma can improve the high temperature strength and slag resistance.

EXPERIMENTAL

MATERIALS

Materials for this study were supplied by Atlas Steels Company and comprised used and unused doloma bricks. A list of the various types of unused doloma bricks with their chemical composition and physical properties is given in Table 1. Four types of commercial doloma refractories - direct-bonded (DBD), tar-bonded (TBD), resin-bonded (RBD), and carbon-containing doloma (CD) - were examined and their compatibility with steel refining slags was determined. The compositions of the slags used are given in Table 2.

MICROSCOPY

Polished sections of the unused and slagged bricks were prepared. Due to the hygroscopic nature of the samples, polishing was conducted in a mixture of alumina and alcohol. Both optical and scanning electron microscopy (SEM) were used to determine the microstructural characteristics of the unused and slagged bricks.

ENERGY DISPERSIVE X-RAY ANALYSIS (EDXR)

Semi-quantitative analysis of the composition changes due to the reaction of the bricks with the slags at high temperature was carried out using energy dispersive x-ray.

X-RAY DIFFRACTION (XRD)

The various phases in the unused and test bricks were identified by means of x-ray diffraction.

CUP TEST

A vacuum furnace was used to test the bricks' resistance to slag corrosion at high temperature. The unused DBD, TBD, RBD and CD bricks were machined into small cylindrical blocks of approximately 3.6 cm in diameter by 3.6 cm in height. A hole of 1.3 cm diameter by 3 cm deep was core drilled at the centre of each block to make a crucible. Five grams of slag sample was packed into each of these refractory crucibles. The crucible and its contents were then loaded into a molybdenum safety crucible, which was in turn placed in the vacuum furnace. After the furnace was evacuated to a pressure of approximately 0.25 Pa, the temperature was increased rapidly to the test temperature and held at that temperature for three hours. Upon completion of the heating cycle, the sample was allowed to cool in the vacuum chamber of the furnace. The test sample was sectioned and polished for optical microscopy (OM), scanning electron microscopy (SEM) and energy dispersive X-ray (EDXR) examination.

RESULTS AND DISCUSSION

MICROSTRUCTURE OF THE UNUSED DOLOMA BRICKS

The microstructures of the as-received dolomas are different. This is particularly noticeable on the fresh fracture surfaces. The most distinguishing characteristic of these materials is the colour of the grog grains, which varied from 2 to 7 mm in diameter and were distributed randomly in a fine-grained matrix. The DBD brick is composed of light brown grog grains in a light to medium gray matrix. The grog grains in the TBD brick are white to grayish and are distributed randomly in a dark gray groundmass. The groundmass of the RBD brick is medium gray, containing white grog grains. The matrix of the CD brick is gray to dark gray, containing randomly distributed 2 to 6 mm diameter gray to dark gray grog grains.

Optical micrographs of the different types of doloma are shown in Fig. 1. In the microstructures of TBD and RBD bricks, the grog grains are loosely bonded by angular to subangular fine-grained matrices and differ from the more tightly bonded fine-grained matrix in the DBD and CD materials. It can be seen that the CD is also bonded by the flake graphite. Under high magnification, the grog grains are seen to be composed of two distinct phases, and distinguishable by their different reflectivity. The highly reflective phase is lime-rich whereas the low reflectivity phase is magnesia-rich.

The microstructures of the dolomas obtained from the SEM microscope are shown in Fig. 2. The compositions of these materials were qualitatively estimated using EDXR analysis which revealed that the grog grains and matrix materials for TBD, RBD and CD bricks are principally MgO and CaO. The matrix of the DBD brick differs from the other dolomas by its appreciably higher MgO content, which is bonded by a calcium silicate phase (Fig. 3).

X-RAY DIFFRACTION OF THE UNUSED DOLOMA BRICKS

XRD of the unused doloma bricks revealed, in addition to the principal lime and periclase, a trace of portlandite ($Ca(OH)_2$) in the TBD, DBD and CD materials. The portlandite phase formed principally by the reaction of the CaO with moisture. A tricalcium silicate phase was detected in the DBD brick.

SLAG CORROSION TESTS

The refractories were tested in contact with slags having $CaO:SiO_2$ ratios (C/S) of 0.96, 1.34 and 3.12 in a vacuum furnace at 1650 to 1700°C for 3 h. The slag resistance of these materials was estimated by the degree of degradation of the microstructure and the new phases developed as a result of slag infiltration.

Characteristics of Dolomas Reacted with Different Slags at Various Temperatures

After contact with different slags at high temperature, the degree of corrosion resistance of the dolomas can be established readily by visual inspection. The test results showed that the principal mechanism of refractory degradation stems from the slag infiltration.

In contact with slag of C/S = 1.34 at 1650°C, both micro- and macrocracks formed in the TBD bricks. Such cracks were not found in the other materials with this slag (Fig. 4).

In contact with slag having C/S = 0.96 at 1700°C, microcracks were developed in all test specimens (Fig. 5).

In contact with slag having C/S = 3.12 at 1700°C, extensive cracks were developed in the TBD brick (Fig. 6), whereas only minor fractures were observed in the other materials.

The micro- and macro-cracks developed in these test samples are attributed to the formation of an unstable dicalcium silicate phase resulting

from the reaction of the slag with the refractories. On cooling, the dicalcium silicate inverted from the beta to the gamma form: this change in morphology is accompanied by a volume increase that stresses the material to the point of failure. XRD was used to determine the various phases in the slag and refractories and confirmed the presence of gamma, beta and alpha dicalcium silicate and tricalcium silicate as the reaction products.

Microstructures of Dolomas Reacted with Slag of C/S = 1.34 at 1650°C

The principal cause of refractory degradation resulting from the slag infiltration through the matrix of the dolomas can be seen in the optical micrographs in Fig. 7. In general, the grog grains are less subject to slag corrosion. However, it does appear that the grog grains in the TBD material are quite susceptible to slag corrosion, as indicated by the degree of dissolution of these grains. It should also be noted that the TBD brick contains a higher concentration of pores in the matrix and a loose bond between matrix and grog grains, which facilitates slag penetration and attack. In contrast, in the highly slag resistant DBD material the micrograph shows that the grog grains are tightly bonded, hence have a reduced surface area of material in contact with the slag. In addition, both the grog grains and matrix material in the DBD are enriched in magnesia, which is slightly higher in slag corrosion resistance.

The microstructure at the slag-brick interface for the CD material is shown in Fig. 8. At the interface, dissolution of CaO occurred as a result of the slag-brick reaction. Based on the EDXR maps for Mg and Si given in Fig. 8, the silica from the slag reacted with the calcium from the brick to form calcium silicate. The MgO thus released from the doloma is either recrystallized as periclase or reacted with the silica from the slag to form magnesium silicate. It can be seen in the micrograph that the graphite is inert and does not react with the slag and thus it acts as a barrier to prevent the slag infiltration into the doloma.

The microstructure of the slag-brick interface of the TBD brick is shown in Fig. 9. Based on the elemental distribution maps of Mg, Si and Ca obtained by EDXR, the reaction between the slag and the brick forms identical phases to those observed for the CD material. It can also be seen that a very sharp slag-brick interface was developed, showing also a thin protective MgO-rich layer formed at the peripheries of the grog grains. It appears that this MgO-rich layer inhibits the slag from further corrosion of the grog grains.

The microstructure and elemental distribution of Ca, Mg and Al for the RBD brick at the slag-brick interface are given in Fig. 10. The micrographs show that the angular to subangular doloma matrices are slag impregnated with Si to form calcium silicate. The magnesium appears to react with the alumina and calcium to form calcium aluminosilicate.

The slag-brick interface of the DBD material is shown in Fig. 11. Evidence of the dissolution of CaO and recrystallization of MgO at the slag-brick interface are readily apparent.

Microstructure of Dolomas Reacted with Slag of C/S = 0.96 at 1700°C

The slag-brick interface for the CD brick, shown in Fig. 12, indicates that the slag dissolved the CaO component from the doloma; the CaO reacted with the silica to form calcium silicate, leaving the MgO to recrystallize in the slag.

The microstructure of the TBD brick at the slag-brick interface is shown in Fig. 13, together with the elemental distribution maps for Mg, Ca and Al. These results indicate that calcium aluminate crystallized at the boundaries of the grog grains and matrix as a result of slag reaction with the refractory.

A well-defined slag-brick interface was developed in the RBD material, as shown in Fig. 14. Based on the elemental distribution maps for Si, Mg and Ca, the principal phases formed were calcium silicate and periclase and these occurred principally in the interstices. Epitaxial growth of periclase on the rim of the doloma grog grains is readily apparent from the Mg distribution map.

The microstructure of the slag-brick interface for the DBD material is given Fig. 15, together with the elemental distribution maps of Ca, Mg and Si. The results reveal that the MgO recrystallized in the slag and grew epitaxially around the grog doloma grains.

Microstructure of Dolomas Reacted with Slag of C/S= 3.12 at 1700°C

In contact with a more basic slag at 1700°C, the phases developed at the slag-brick interface for the different dolomas are principally calcium silicate, calcium magnesium silicate and a lesser amount of calcium magnesium aluminate.

The microstructure of the CD material at the slag brick interface and the silica distribution map given in Fig. 16 indicate that calcium silicate crystallized at the grain boundaries and the matrix of the doloma, leaving the graphite flakes unreacted and forming barriers to prevent further slag infiltration.

The microstructure of the DBD slag-brick interface shown in Fig. 17 is not very well defined. The principal phase formed by the reaction of the slag with the bricks is calcium magnesium aluminate, as shown by the elemental distribution maps.

Microstructure of the slag-brick interface for the TBD material and the elemental distribution maps given in Fig. 18 reveal that the MgO component recrystallized in the slag with calcium silicate occurring in the interstices.

The principal phase formed at the slag-brick interface for the (RBD) material is calcium silicate, as indicated by the SEM micrograph and the elemental distribution maps (Fig. 19).

Characterization of the Used Bricks from the Ladles

The microstructure of the used RBD bricks from the steel ladles were examined by SEM and EDXR techniques. SEM micrographs of the slag-brick interface for bricks after 1 and 49 heats respectively are given in Fig. 20 and 21. The mechanism of chemical attack on the doloma particles is similar to the test cups, with preferential dissolution of the CaO crystals to the slag and release of the MgO into the slag at the working face. Also visible is the presence of grapnite at the brick-slag interface for the brick subjected to 1 neat. This suggests that carbonaceous materials formed from the resin bond, which migrated into the brick, and this carbon-rich zone subsequently graphitized. The absence of graphite after 49 heats suggests that, with time, a gradual decrease occurs in the grapnite content at the slag-brick interface due to decarburization or oxidation. Figure 22 shows the slag infiltration confined mainly along the grain boundaries of the doloma and along the platelets of the graphite crystals. It has been demonstrated that the graphite is highly slag resistant due to the non-wetting character of the material.

CONCLUSIONS

The corrosion of doloma refractories by different slags was evaluated in the laboratory. Examination of the test specimens and specimens removed from a secondary steelmaking ladle have shown the following failure mechanism:

1. An increase in slag acidity results in an increase in refractories wear of all types of doloma bricks examined. With the highly basic slag, the dissolution of both MgO and CaO is small.
2. All dolomas exhibited excellent corrosion resistance to highly basic slag at temperatures below 1700°C, as indicated by the shallow slag penetration and the few micro- or macro-cracks formed.
3. The grog grains have higher slag corrosion resistance than the matrix, due to their higher density and lower porosity.
4. The temperature dependence of the corrosion is large for the TBD brick. It has been observed that at temperatures above 1700°C, substantial slag infiltration occurred, resulting in rapid degradation of the doloma; this is a function of the relatively higher porosity of the matrix. This type of brick is considered the least desirable for this service.
5. The slagging retarding action of graphite is readily apparent in the CD and RBD materials. Graphitization of the resin in RBD brick appears to negate the expected weakness owing to loose bonding. These types are considered preferable for this service.
6. Another factor that may have important bearing in using these bricks is their susceptibility to hydration, which limits their shelf-life.

ACKNOWLEDGEMENTS

The writers wish to express their thanks to Atlas Steels Company for supplying the necessary materials for this study. Thanks are also due to G. Lemieux for his assistance in the experimental work, to Y. Bourgoin for preparation of polished sections and to D. Owen for the SEM microscope work.

REFERENCES

1. Whittaker, D.A. and Palmer, A.R. "Ladle metallurgy at Welland plant of Atlas Steels"; I&SM 31-35; June 1981.

2. Gilpin, W.C. and Spencer, D.R.F. "New development in dead burnt magnesite and dead burnt dolomite"; Refract J 4:4-20; 1972.

3. Evan, J.L. "Furnace design and operations - key to refractory performance"; Refract J 9-21; Oct. 1980.

4. Spencer, D.R.F. "Basic refractory raw materials"; Trans Br Ceram Soc 71:123-134; 1972.

5. Alcock, S. and Spencer, D.R.F. "The application and performance of basic refractories in secondary steelmaking ladles"; Trans Br Ceram Soc 77:45-57; 1978.

6. Carswell, G.P., Crosby, M.P. and Spencer, D.R.F. "Development of high performance ladle linings"; Refract J 9-21; Jan-Feb. 1980.

7. Knoche, C.H., Koltermann, M. and Stolte, G. "Refractories for vacuum steelmaking"; Trans Br Ceram Soc 76:141-148; 1977.

8. Doman, R.C., Barr, J.B., McNally, R.N. and Alper, A.M. "Phase equilibria in the system CaO-MgO"; Bull Am Ceram Soc 46:313-316; 1963.

Table 1 - Physical and chemical properties of the unused doloma bricks

	Direct Bonded (DBD)	Tar Bonded (TBD)	Resin Bonded (RBD)	Carbon Containing (CD)
MgO %	36	36	41	
CaO %	61	61	57	
SiO_2 %	1.5	1.0	0.6	
Al_2O_3 %	1.0	1.0	0.4	N/A
Fe_2O_3 %	1.0	1.0	1.0	
Total porosity vol %	17-21	8-12	15-16(ignited)	
Cold crushing strength, N/mm^2	40	30	-	
Density @20°C, kg/m3	2700-2850	2800-2950	2810-2960	

Table 2 - Chemical compositions of the slag samples

	SiO_2	Cr_2O_3	Al_2O_3	CaO	MgO	Fe_2O_3	CaO:SiO_2
T1	33.30	0.63	10.50	44.80	9.81	0.97	1.34
T2	38.15	0.43	10.04	36.59	12.79	0.94	0.96
VAD	19.20	0.02	10.11	60.06	3.69	3.12	3.12

*T1 slag in contact with refractories at 1650°C for 3 h.
T2 slag in contact with refractories at 1700°C for 3 h.
VAD slag in contact with refractories at 1700°C for 3 h.

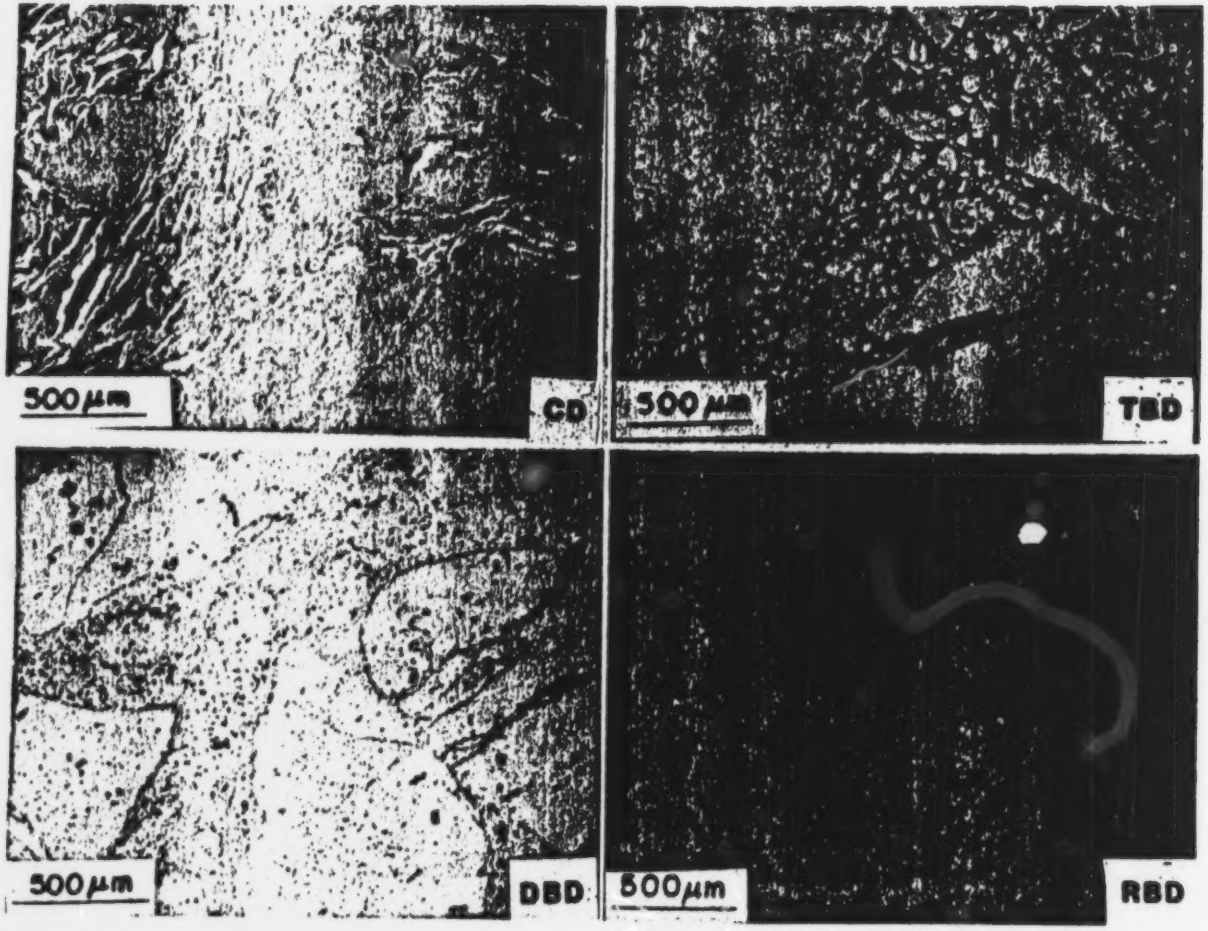

Fig. 1 - Optical micrographs showing the microstructures of the unused bricks

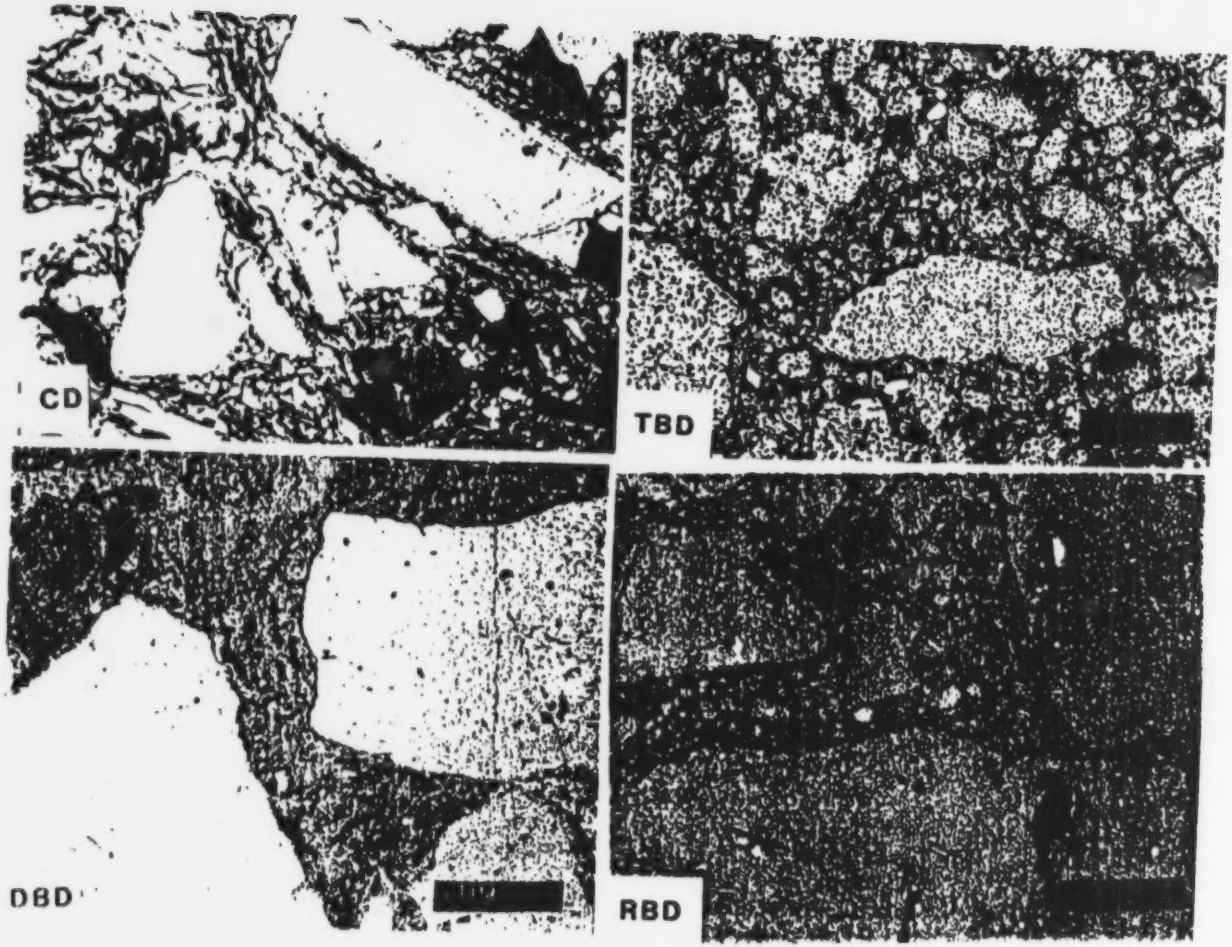

Fig. 2 - SEM micrographs showing the microstructures of the unused bricks

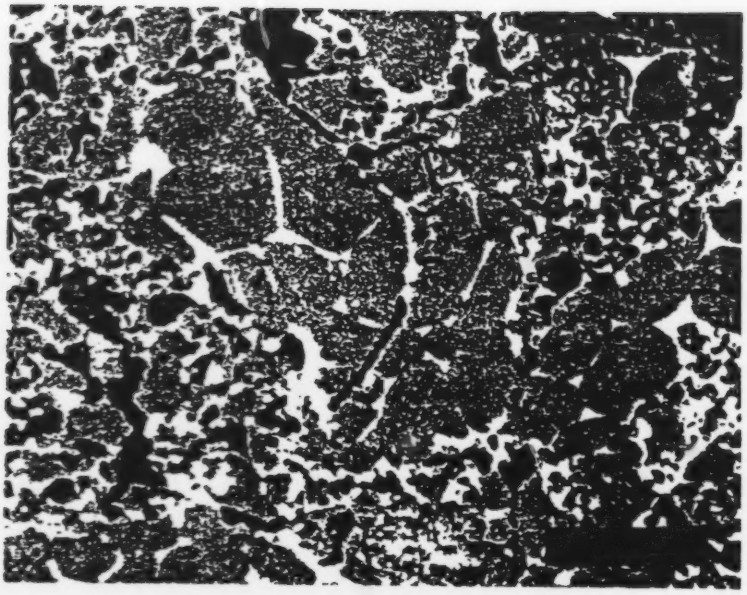

Fig. 3 - SEM micrograph showing the calcium silicate phase of the grain boundaries of the unused DBD brick

Fig. 4 - The appearance of test cups from different types of bricks in contact with C/S slag = 1.34 at 1650°C for 3 h

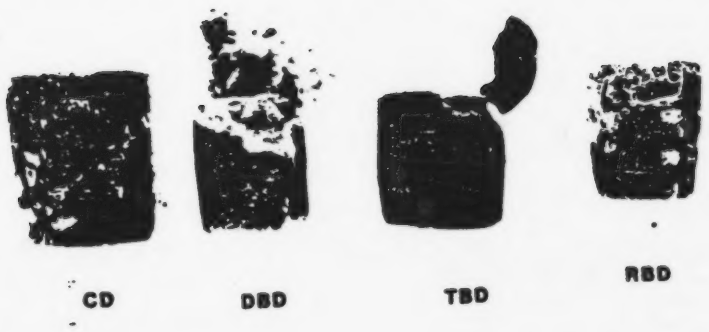

Fig. 5 - The appearance of test cups from different types of bricks in contact with C/S slag = 0.96 at 1700°C for 3 h

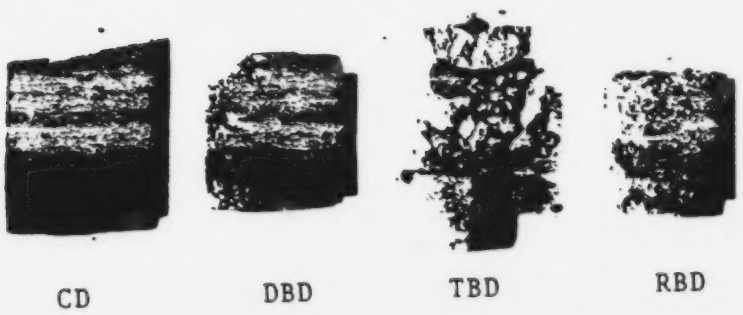

Fig. 6 - The appearance of the test cups from different types of bricks in contact with slag of C/S = 3.12 at 1700°c for 3 h

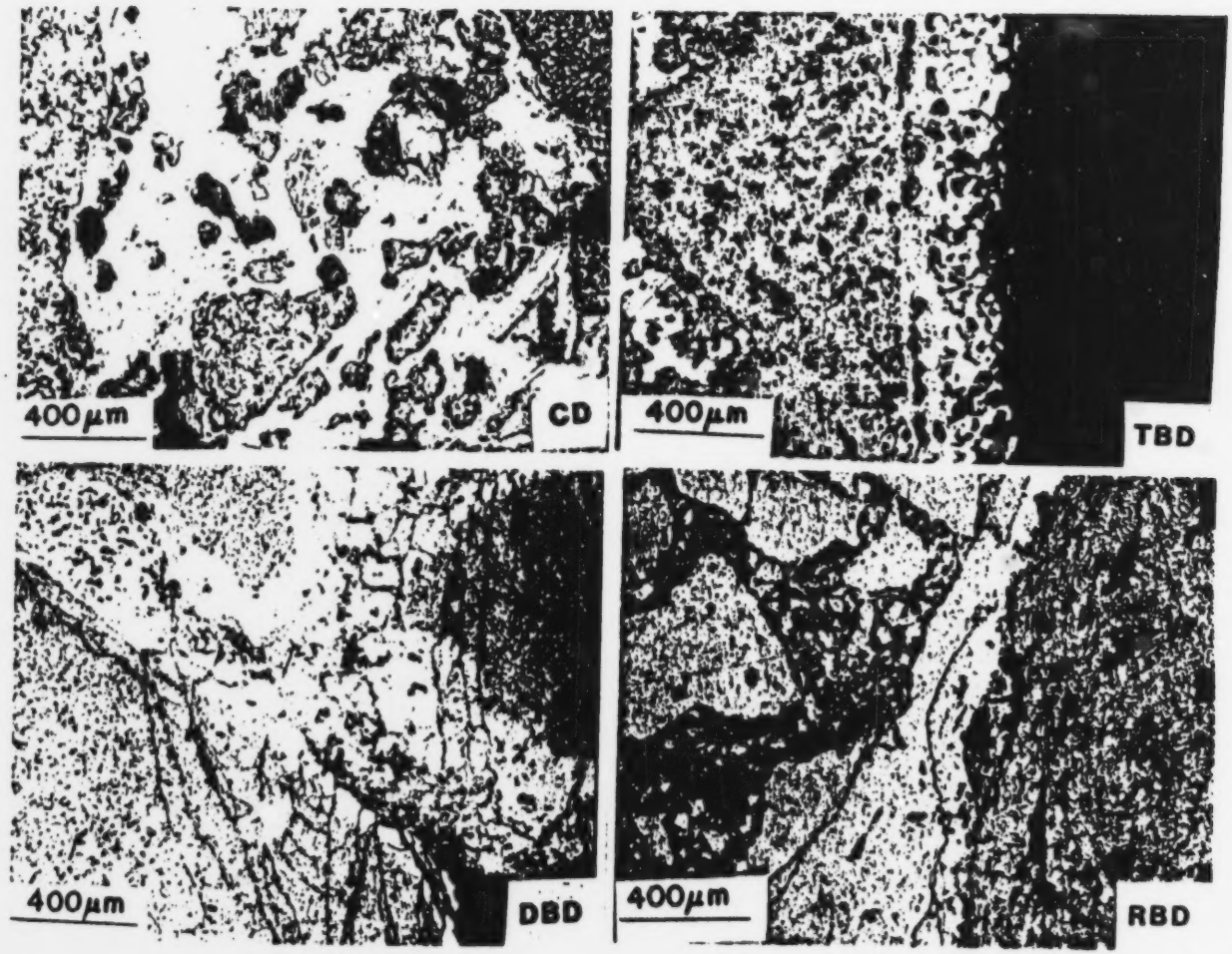

Fig. 7 - Optical micrographs at the slag-brick interface of different refractories

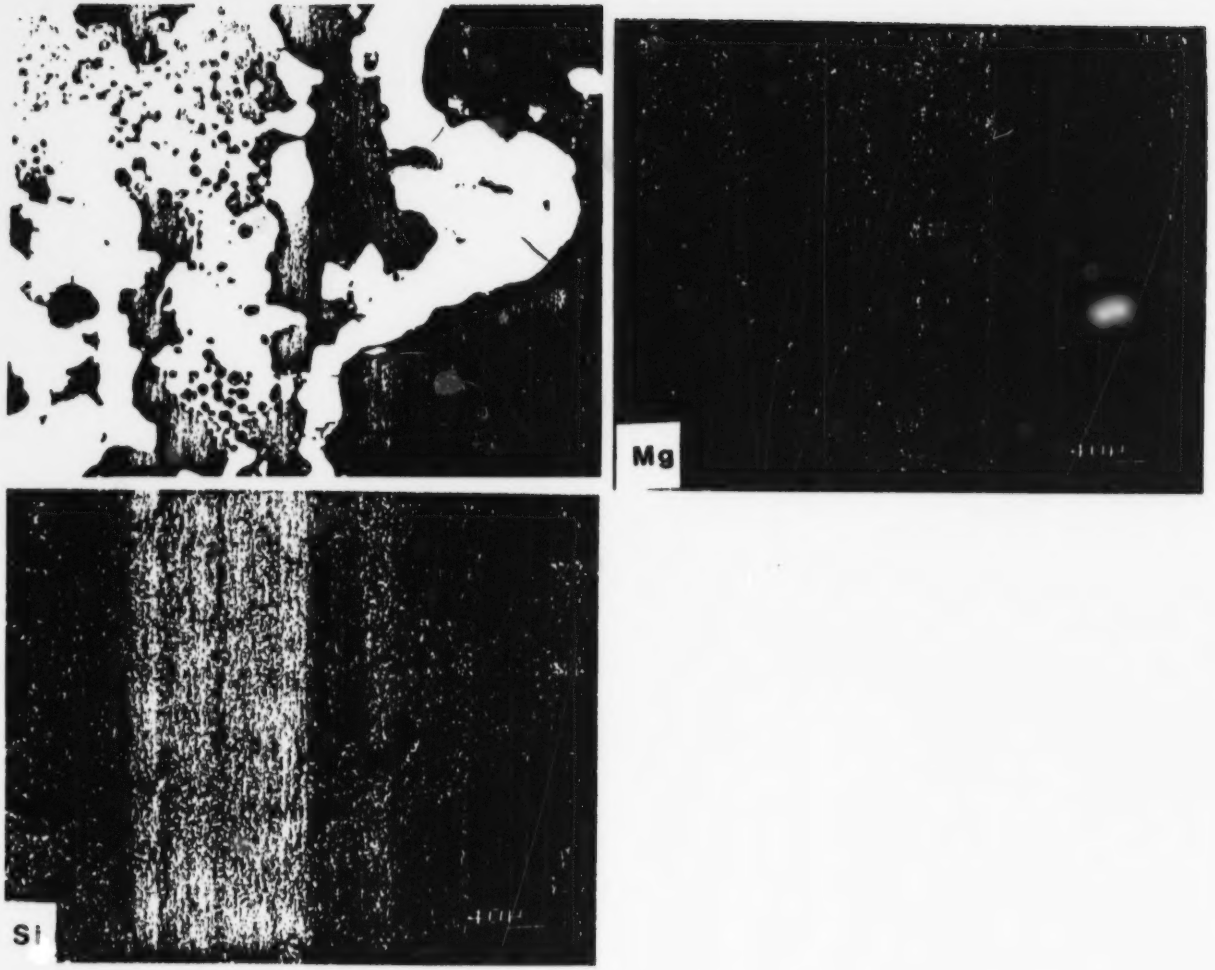

Fig. 8 - SEM micrograph of the CD brick in contact with slag and elemental distribution maps for Mg and Si

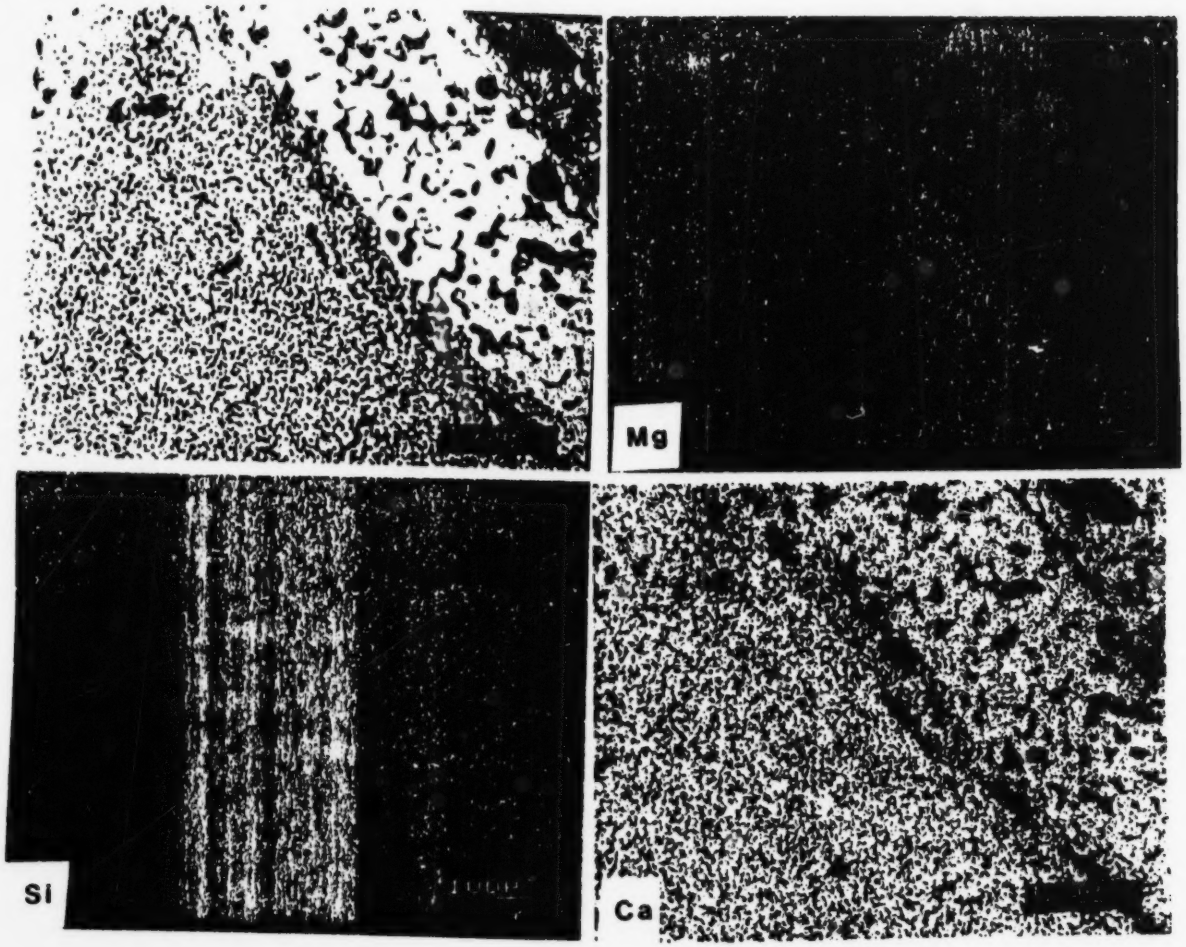

Fig. 9 - SEM micrograph of slag infiltrated TBD brick and EDXR maps showing elemental distributions

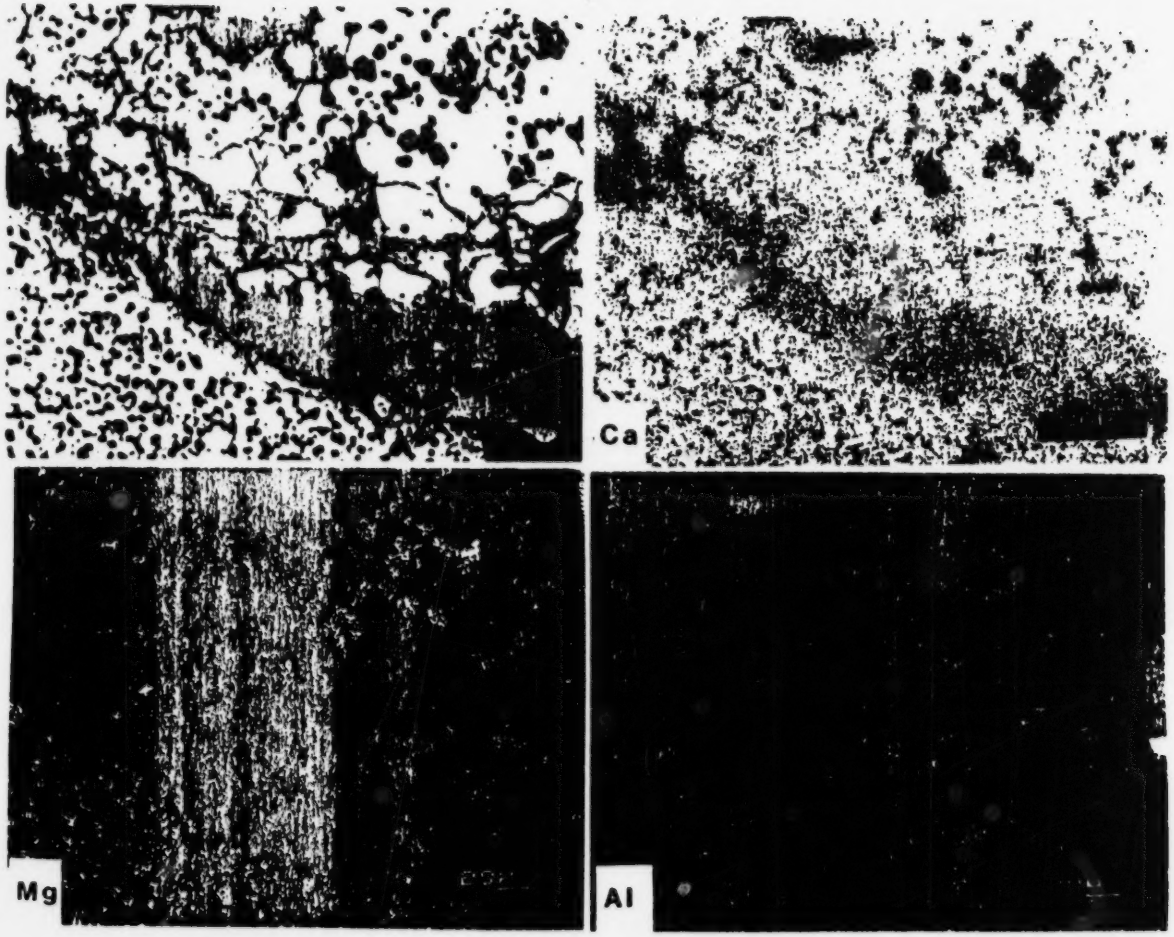

Fig. 10 - SEM micrograph of slag infiltrated RBD brick and EDXR maps showing elemental distributions

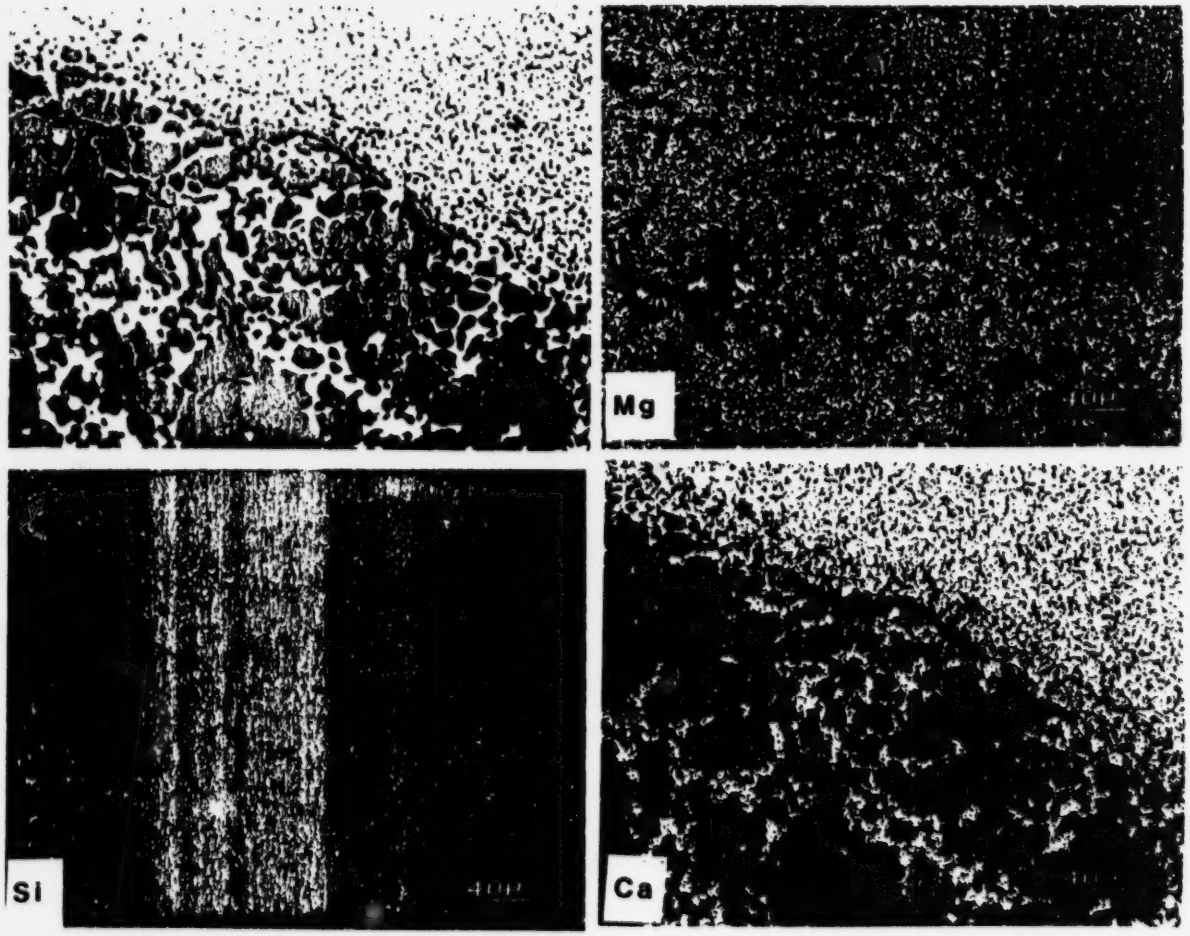

Fig. 11 - SEM micrograph of slag infiltrated DBD brick and EDXR maps showing elemental distributions

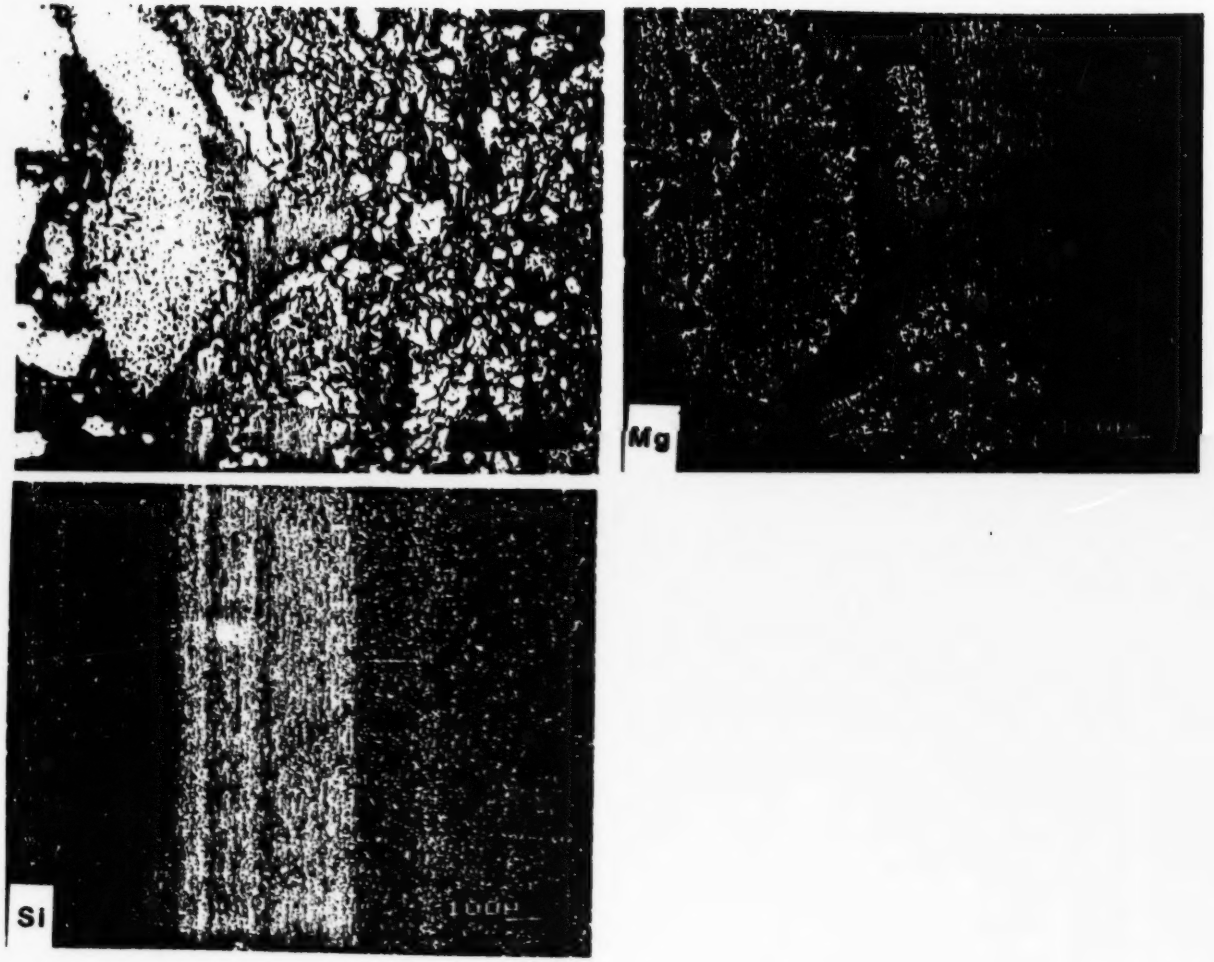

Fig. 12 - SEM micrograph of slag infiltrated CD brick at 1700°C and EDXR maps showing elemental distributions

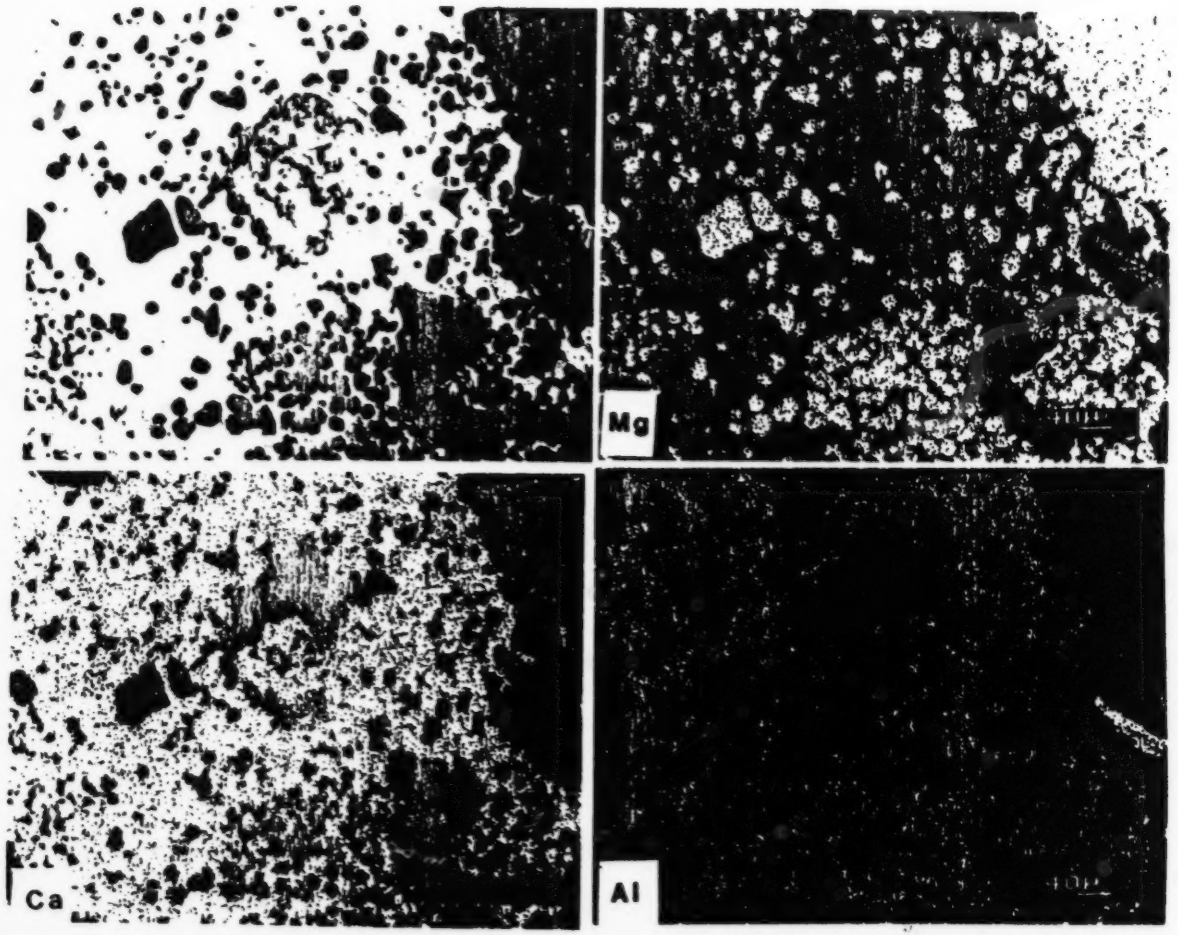

Fig. 13 - SEM micrograph of slag infiltrated TBD brick at 1700°C and EDXR maps showing elemental distributions

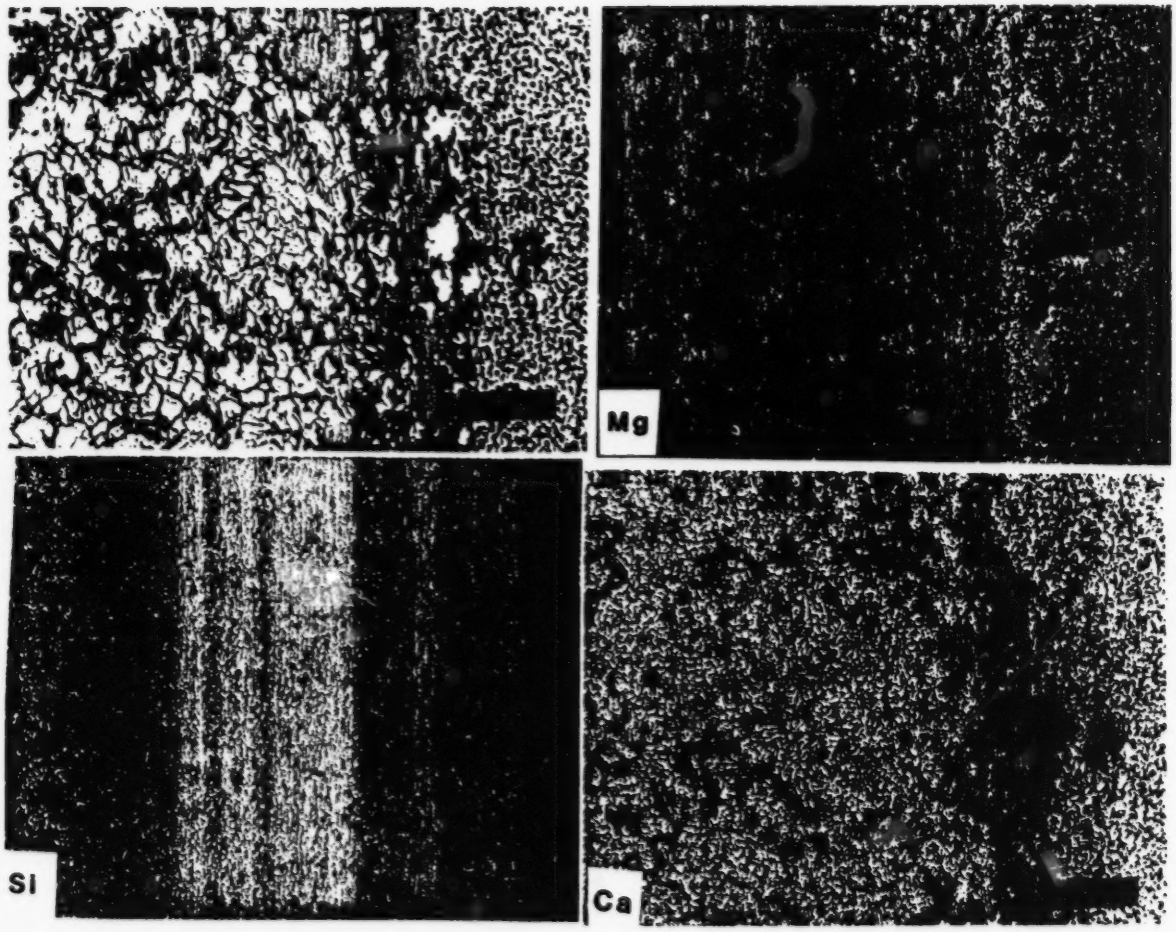

Fig. 14 - SEM micrograph of slag infiltrated RBD brick at 1700°C and EDXR maps showing elemental distributions

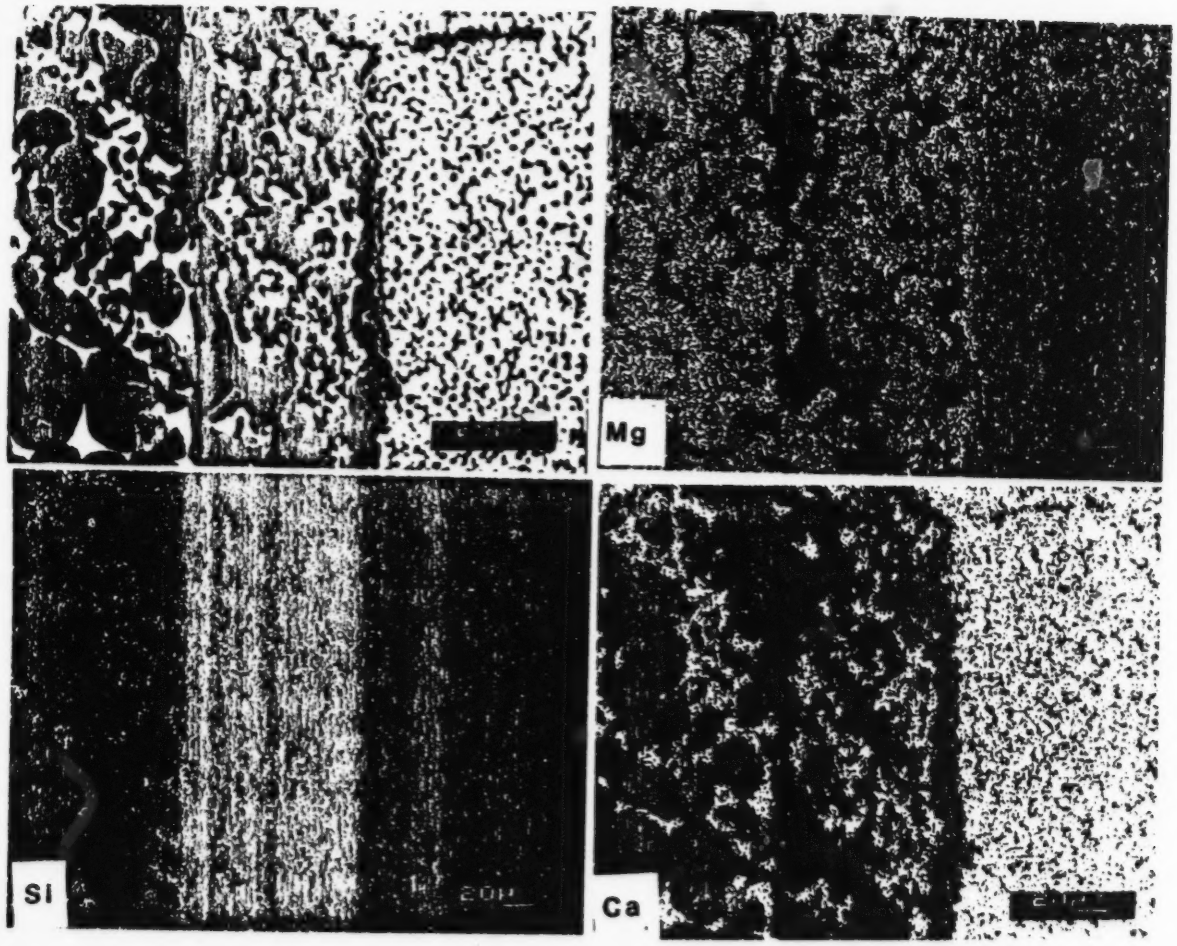

Fig. 15 - SEM micrograph of slag infiltrated RBD brick at 1700°C and EDX maps showing elemental distributions

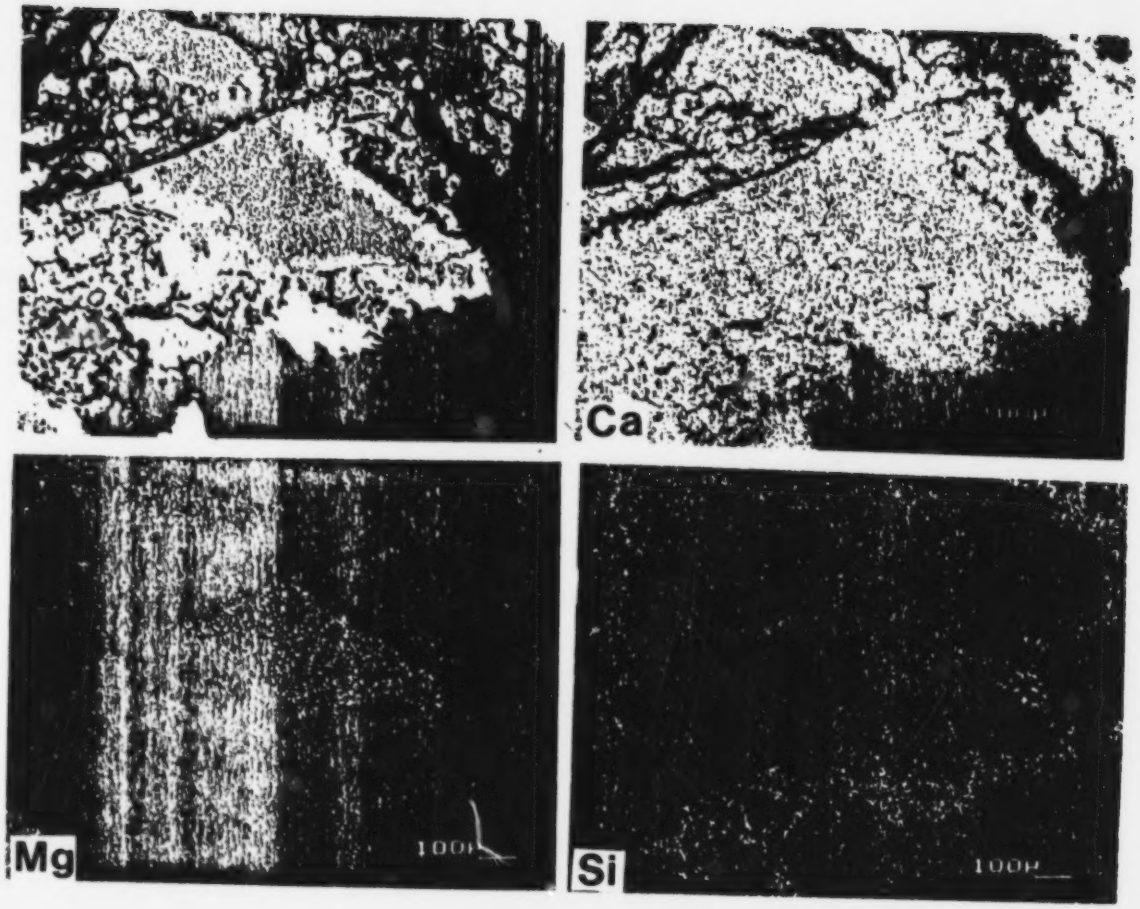

Fig. 16 - SEM micrograph of slag infiltrated CD brick and EDXR maps showing elemental distributions

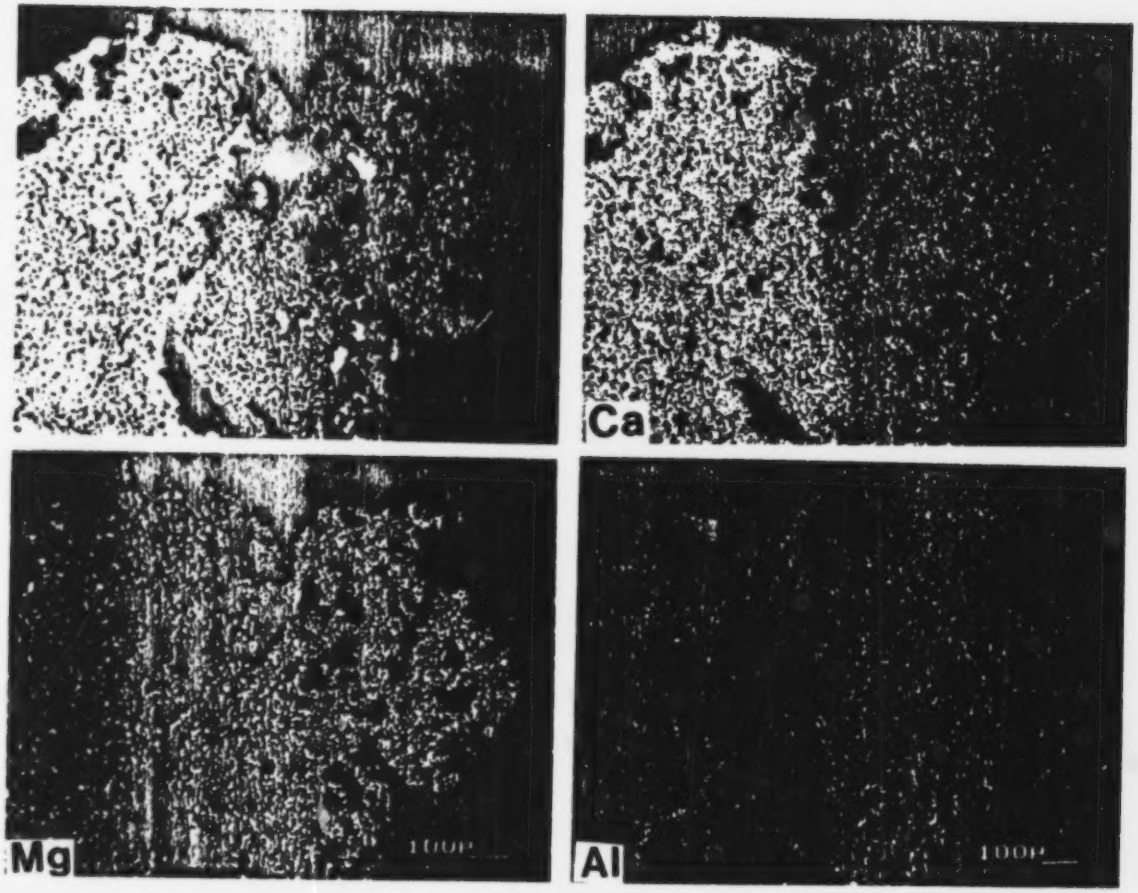

Fig. 17 - SEM micrograph and EDXR maps of Ca, Mg and Al for DBD brick reacted with C/S slag = 3.14 at 1700°C

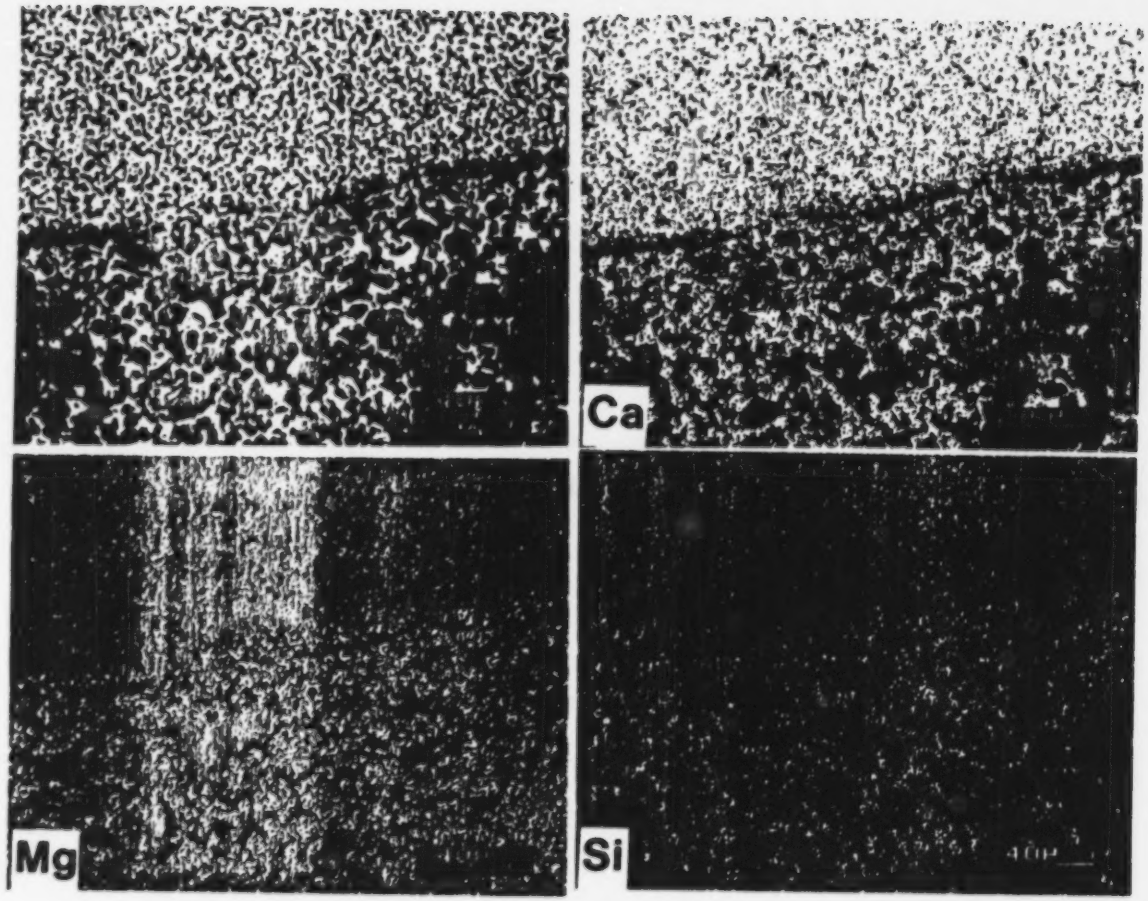

Fig. 18 - SEM micrograph and EDXR maps of Mg, Ca and Si for TBD brick reacted with C/S slag = 3.14 at 1700°C

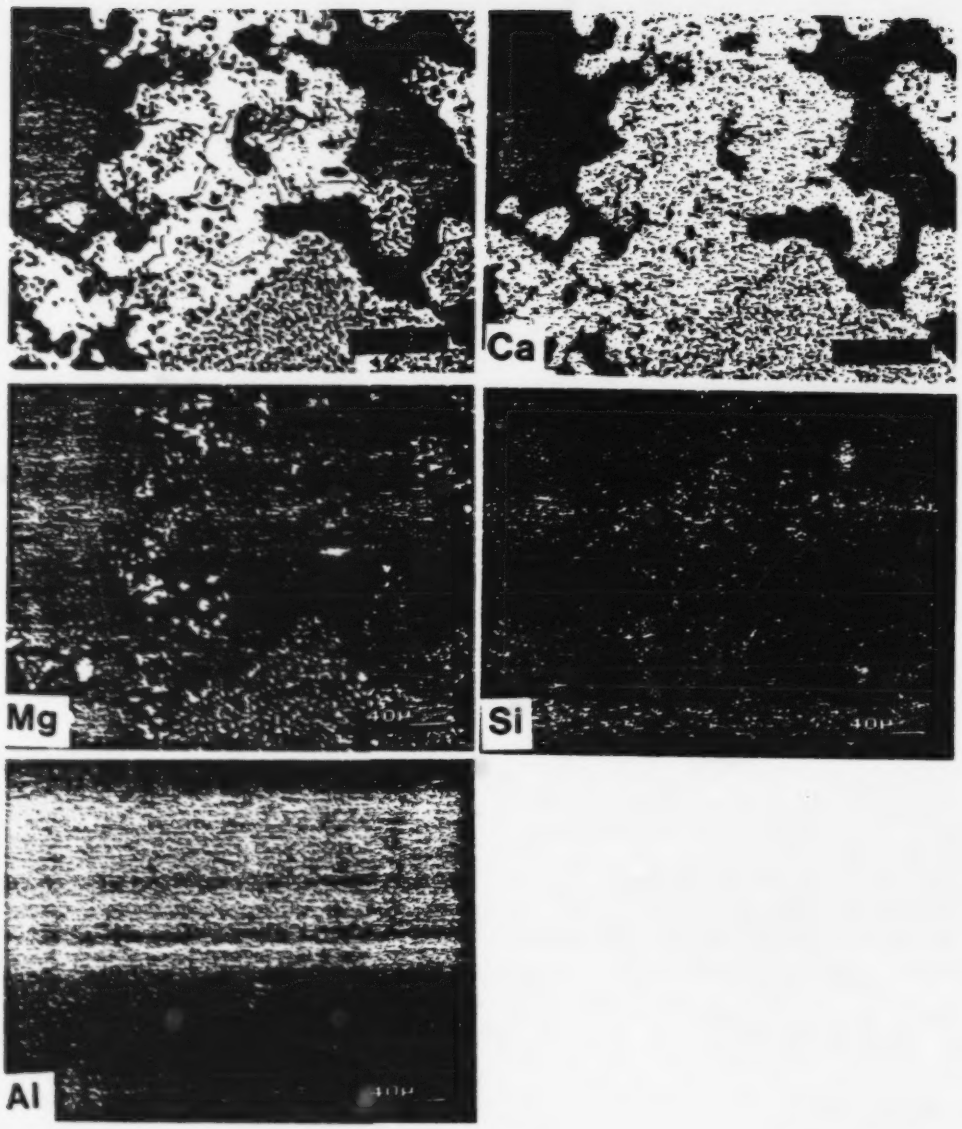

Fig. 19 - SEM micrograph and EDXR maps of Mg, Al, Ca and Si reacted with C/S slag = 3.14 at 1700°C

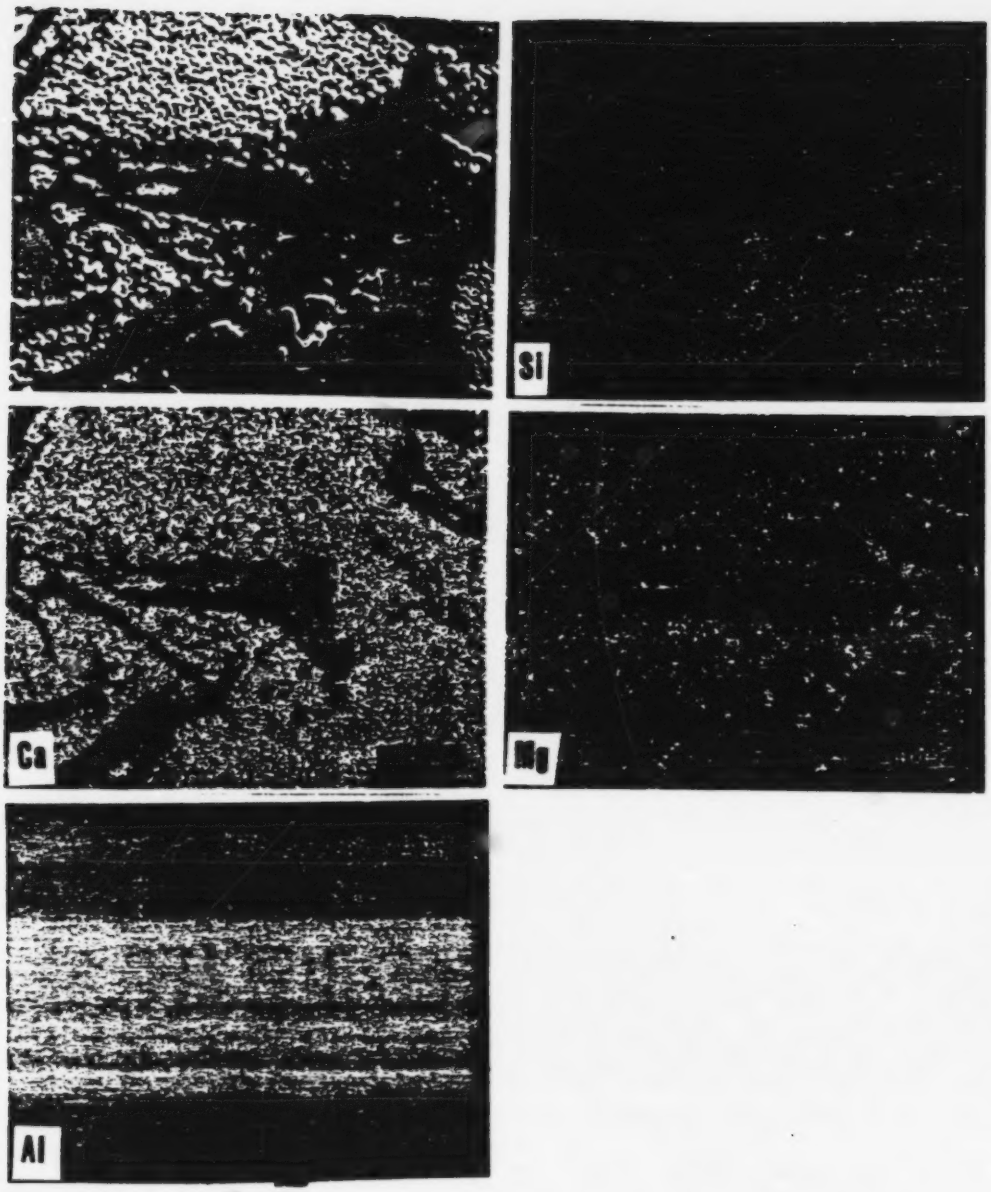

Fig. 20 - SEM micrograph of the used RBD brick from ladle after 1 heat and EDXR maps showing elemental distributions

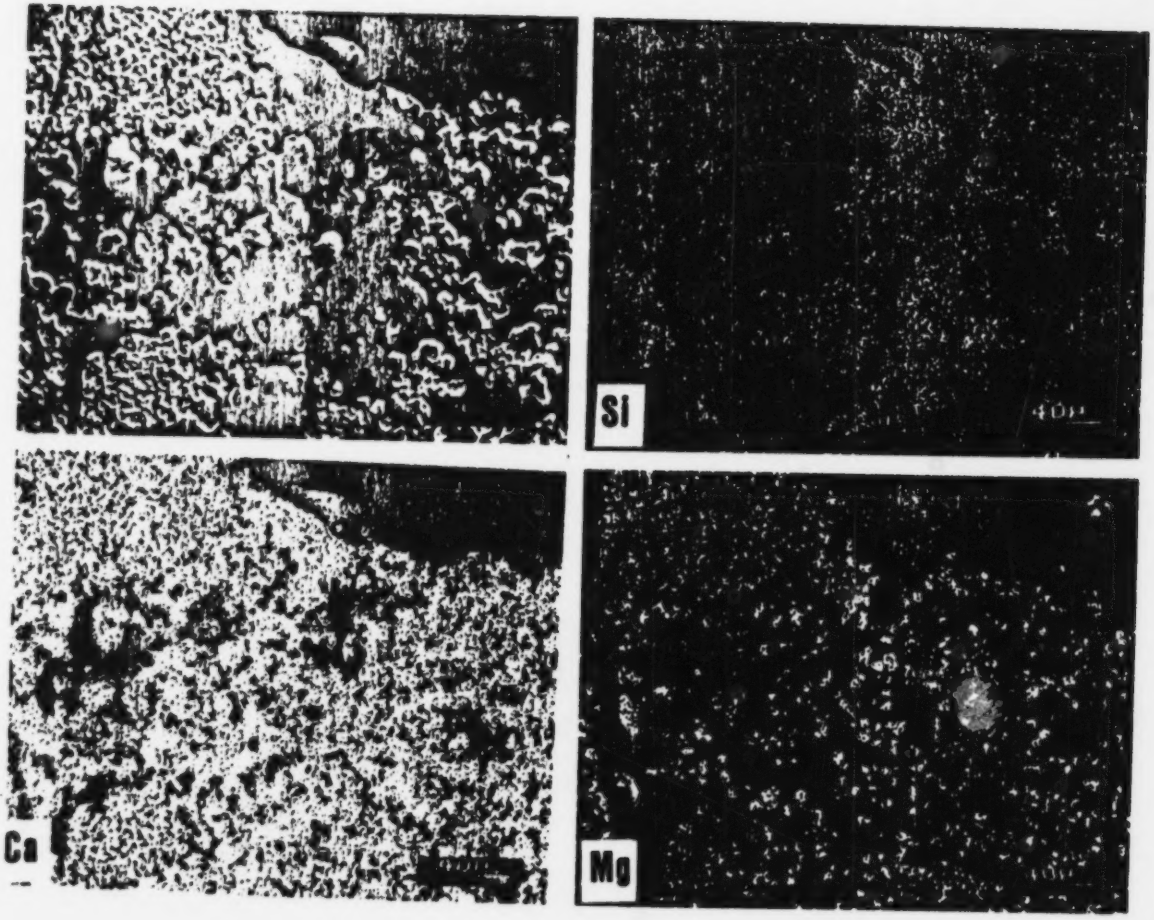

Fig. 21 - SEM micrograph of the used RBD brick from ladle after 49 heats and EDXR maps showing elemental distributions

Fig. 22 - Optical micrograph of the a RBD brick after 1 heat